Journal of the Physical Society of Japan **85**, 124403 (2016)
http://doi.org/10.7566/JPSJ.85.124403

Generation of Narrow-Band Polarization-Entangled Photon Pairs at a Rubidium D1 Line

Long Tian[1,2], Shujing Li[1,2*], Haoxiang Yuan[1,2], and Hai Wang[1,2†]

[1]*The State Key Laboratory of Quantum Optics and Quantum Optics Devices, Institute of Opto-Electronics, Shanxi University, Taiyuan 030006, People's Republic of China*
[2]*Collaborative Innovation Center of Extreme Optics, Shanxi University, Taiyuan 030006, People's Republic of China*

(Received August 18, 2016; accepted October 20, 2016; published online November 17, 2016)

Using the process of cavity-enhanced spontaneous parametric down-conversion (SPDC), we generate a narrow-band polarization-entangled photon pair resonant on the rubidium (Rb) D1 line (795 nm). The degenerate single-mode photon pair is selected by multiple temperature controlled etalons. The linewidth of generated polarization-entangled photon pairs is 15 MHz which matches the typical atomic memory bandwidth. The measured Bell parameter for the polarization-entangled photons $S = 2.73 \pm 0.04$ which violates the Bell-CHSH inequality by ∼18 standard deviations. The presented entangled photon pair source could be utilized in quantum communication and quantum computing based on quantum memories in atomic ensemble.

1. Introduction

Storage of entangled photons is a key component for long-distance communication and linear quantum computation.[1–6] Spontaneous parametric down-conversion (SPDC) in nonlinear crystals is the most widely used method to generate entangled photons.[7–10] However, the entangled photons from single-pass SPDC have a very broad linewidth on the order of THz[8,9] which are unfeasible to be stored in the most matter nodes.[2,11–14] For instance, the typical bandwidths of the atomic quantum memories range from MHz to GHz.[14–18] In order to efficiently store the entangled photons in atomic memories, we need to reduce the linewidth of entangled photons from SPDC.

By means of optical filters, the linewidths of the photons from SPDC have been reduced to GHz even MHz order and the storages of the entangled photons have been demonstrated in solid-state[11,12] and atomic ensembles.[14] The drawback of the filtering scheme is that the count rate of photons is inevitably decreased. For solving this problem, cavity-enhanced SPDC has been developed to prepare the narrow-band photon pairs.[19] By putting the nonlinear crystal inside a cavity, the linewidth of generated photon pairs is limited by the cavity linewidth and the generation probability for the down-converted photons whose frequency matches the cavity mode will be enhanced greatly. Significant progress has been made in this regard.[19–25] Recently, the generation of single-mode narrow-band polarization entangled source has been reported through cavity-enhanced SPDC,[25] and the storage of such entangled photons has been demonstrated in a cold atomic ensemble.[26]

In this paper, we also demonstrate a narrow-band polarization-entangled photon pairs at Rb D1 line (795 nm). Based on cavity-enhanced SPDC, a pair of horizontally (H) and vertically (V) polarized photons is generated from a type-II periodically poled $KTiOPO_4$ (PPKTP) crystal placed in a cavity. Passing though multiple etalons, the non-degenerate correlated photon pairs from the cavity are filtered and the degenerate single-mode pairs are remained. The single-mode photon pair is split into two parts with a 50/50 non-polarizing beam splitter (NPBS). For the case that each output port has one photon, the photon pair will be in polarization entangled state in the post-selected manner. In contrast to the past experiment,[25] in which, $|H\rangle$ and $|V\rangle$ modes of the photon pairs are separated on a polarizing beam splitter (PBS), and filtered by two different etalons, respectively, then combined on another PBS for generating entangled photon pairs, in our experiment, the $|H\rangle$ and $|V\rangle$ modes of the photon pairs are filtered by a set of etalons, and then sent to an 50/50 NPBS to generate entangled two polarization qubits. So our experimental setup is relative simple. The linewidth of polarization-entangled photon pairs here is 15 MHz, which matches the typical atomic memory bandwidth.[2] The measured Bell parameter $S = 2.73 \pm 0.04$ which violates the Bell-CHSH inequality by ∼18 standard deviations. The coherent length is measured to be about 20 m via a Mach–Zehnder (MZ) interferometer.

2. Experimental Setup

The experimental setup is shown in Fig. 1. A tapered amplifier (TA) is employed to amplify the output power of diode laser which is locked to the D1 line of Rb, the corresponding wavelength is 795 nm. The linewidth of diode laser amplified by TA is less than 1 MHz. The beam from the TA is phase modulated by an electro-optic modulator. This modulation is used to lock a cavity for frequency doubler and a cavity for SPDC via a Pound–Drever–Hall (PDH) locking method.[27] Most of laser is sent to a frequency doubler for generating the 397.5 nm ultraviolet (UV) laser which is used to pump the nonlinear crystal to generate SPDC photon pairs (795 nm), and a small fraction of laser is split as the locking beam of cavity for SPDC.

The frequency doubler is in a standing-wave cavity configuration. A 10 mm long type-I PPKTP crystal is used for second-harmonic generation. By pumping 450 mW of light at 795 nm, we obtain 100 mW of 397.5 nm UV light. The UV light with linewidth of about 1 MHz is used as the pumping beam for SPDC cavity. The cavity for SPDC is also in a standing-wave cavity configuration composed of two concave mirrors with curvature radius 50 mm. The cavity is near concentric in which the distance between two cavity mirrors is 92 mm. The input coupler mirror is high-reflection coated at 795 nm ($R > 99.9\%$) and anti-reflection (AR) coated at 397.5 nm. The output coupler mirror has a

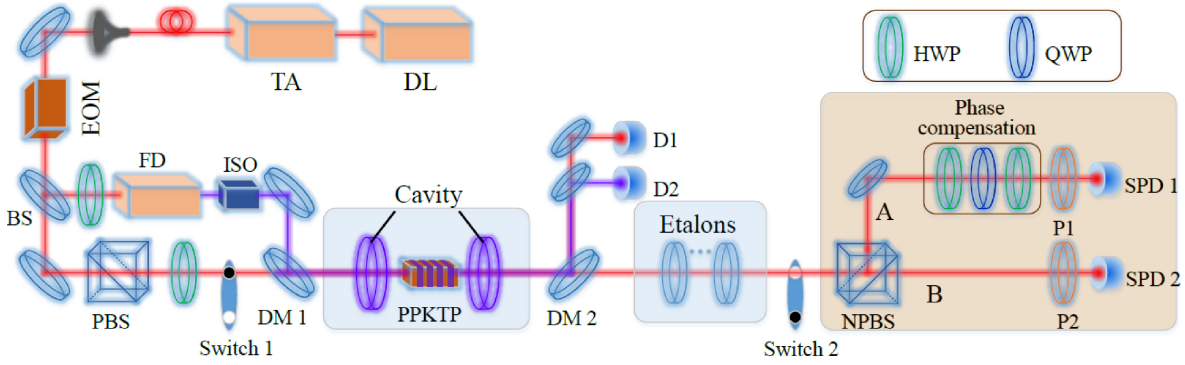

Fig. 1. (Color online) Experimental set-up. EOM: electro-optic modulator; FD: frequency doubler; ISO: optical isolator; DM1–2: dichroic mirrors; NPBS: non-polarizing beam splitter; HWP: half wave plate; QWP: quarter wave plate; P1–2: polarizers; D1–2: photodetectors; SPD1–2: single photon detectors; Switch1–2: mechanical switches.

transmittance of 5% at 795 nm and high reflectance at 397.5 nm. The linewidth of pump beam is smaller than that of the SPDC cavity (about 15 MHz). A 10 mm long type-II PPKTP crystal is used as the down-converter. Under the condition of phase matching, an H polarized UV pump photon down-converts to a near-infrared photon pair (795 nm) with one polarized in H and the other in V. The facets of the PPKTP are AR coated at 795 and 397.5 nm to minimize losses within the cavity. So the SPDC photons are resonant with the cavity and the UV pump light interacts twice with the PPKTP in the cavity. The purpose of UV light interacting twice is to facilitate the mode-matching between UV light beam and the cavity. The temperature of the type-II PPKTP crystal is controlled by a high performance temperature controller with precision of 0.002 °C. An isolator is inserted between the cavity for SPDC and frequency doubler to prevent the reflection of the cavity for SPDC from feeding back to the frequency doubler. We use a dichroic mirror DM1 to combine the locking light with the UV light before the cavity. After the cavity, DM2 is used to separate the residual UV light from the generated down-converted near-infrared photons. The near-infrared light transmits and the UV light reflects on DM2. Due to imperfect coating of DM2, there is a small fraction of near-infrared light in the reflective beam. The near-infrared light is extracted and detected by detector D1 which is used to observe the transmitted signal of cavity and lock the cavity. The cavity is locked at resonance using locking beam via PDH method, and the modulation frequency is 20 MHz. The frequency of degenerate mode (ω_0) of the SPDC photons is as same as that of the locking beam. In order to realize the double resonance of H and V modes in the OPO, the polarization of locking beam is set at 45° by rotating a half wave plate (HWP) so that the both modes can be shown by oscilloscope. By slightly changing the temperature of type-II PPKTP, the peaks of H and V modes are becoming overlapped. The doubly resonant geometry of OPO for H and V polarization is achieved when the peak reaches the maximum height, the temperature of PPKTP is around 40.356 °C. The locking beam with 45° polarization is locked at the maximum height which implies the H and V polarization components are locked at cavity resonance at the same time. Besides, two mechanical switches are used to alternate the periods of cavity locking and signal detection to avoid damaging the single photon detectors (SPDs) and eliminate the background count. The locking repetition rate is 20 Hz.

Due to the large phase-matching bandwidth of SPDC process (300 GHz), there are numerous non-degenerate correlated photon pairs together with degenerate photon pair. The quantum state from the cavity output can be expressed as[25)]

$$\begin{aligned}|\psi\rangle = {} & \sqrt{\chi_0}|\omega_0\rangle_H|\omega_0\rangle_V \\ & + \sum_{m=1}^{N=100} \frac{\sqrt{\chi_m}}{2}(|\omega_0 + m\Omega_H\rangle_H|\omega_0 - m\Omega_H\rangle_V \\ & + |\omega_0 - m\Omega_H\rangle_H|\omega_0 + m\Omega_H\rangle_V \\ & + |\omega_0 + m\Omega_V\rangle_H|\omega_0 - m\Omega_V\rangle_V \\ & + |\omega_0 - m\Omega_V\rangle_H|\omega_0 + m\Omega_V\rangle_V) \end{aligned} \quad (1)$$

with

$$\frac{\chi_m}{\chi_0} = \frac{4}{1 + \frac{4F^2}{\pi^2}\sin^2\frac{m\Delta\Omega}{\Omega}\pi},$$

where Ω_H and Ω_V are the free spectrum ranges (FSR) for H and V modes, respectively. The measured values of Ω_H and Ω_V are 1468 and 1481 MHz, with a difference $\Delta\Omega = \Omega_H - \Omega_V = 13$ MHz. Ω is the average of Ω_H and Ω_V. $F \approx 100$ is the finesse of the cavity. N is determined by the phase-matching bandwidth and the FSR of the cavity. In Eq. (1) only single photon-pair events are considered, and the vacuum states and multiple photon-pairs events are omitted. The first term of the right side of Eq. (1) is the expected degenerate pair output. The following four terms in the summation correspond to the case that one photon is resonant with the cavity while the other is not. The ratio between the summation of these non-degenerate modes to the degenerate mode is

$$\mu = \sum_{m=1}^{100} \frac{\chi_m}{\chi_0} = 1.87.$$

To filter the non-degenerate photon pairs, we employ five Fabry–Perot etalons, including two 5.4-mm-long, two 7.5-mm-long etalons and one 2.1-mm-long etalons. The reflectivities of two surfaces for all etalons are 90% and the measured finesses of them are ~25. The transmitted frequency of these etalons is tuned to the frequency ω_0 of

degenerate photons by controlling their temperatures. Those etalons can keep stable operation in 10 h. The slight reflection from the etalons will cause the OPO cavity to be very unstable. By adjusting the incident angles of light on etalon surfaces to slightly deviate from normal incidence, the feedback to OPO can be avoided and a high transmissivity of degenerate mode can be kept simultaneously. The total transmittance of the five etalons is ~40%. After the filters, the ratio μ is changed from 1.87 to 5.4×10^{-6}.

The degenerate single-mode photon pair is split into two parts with a 50/50 NPBS. Each photon of the photon pair has same probability to be transmitted or reflected at the NPBS. The reflected and transmitted photons are further coupled into two multimode fibers and detected by two SPDs (Perkin-Elmer SPCM-AQRH-15-FC) respectively. The signals from the SPDs are acquired by a four-channel event time digitizer (FAST Com Tec P7888) and analyzed by a computer. If two photons are detected by the two SPDs at the same time, respectively, the two photons are projected into entanglement state: $|\varphi\rangle = (1/\sqrt{2})(|H\rangle|V\rangle - e^{i\alpha}|V\rangle|H\rangle)$,[21] where α is the phase shift between $|H\rangle$ and $|V\rangle$ modes on the NPBS. In order to generate the maximum entanglement state $|\varphi\rangle = (1/\sqrt{2})(|H\rangle|V\rangle - |V\rangle|H\rangle)$, the phase shift is needed to be compensated. We add a phase compensation unit including two quarter wave plates (QWP) and one half wave plate (HWP) in one output path to compensate the phase shift.

3. Results and Discussion

We firstly measured the generation rate of entanglement photon pairs as a function of the UV pump power. In the measurement, the polarization angles of photon A and B are set to 0 and $\pi/2$, respectively. The measured coincidence counts are shown in Fig. 2. The data is fitted with a linear function which is agreed well with experimental data. Because the coincidence counts are measured after projection, the pair generation rate is twice the coincidence counts. We get a maximal generation rate of $1434\,\mathrm{s}^{-1}$ at the pump power of 32 mW. By improving the efficiency of the filters and employing longer nonlinear crystal, the generation of entangled photon pairs can be increased further.

We make a polarization correlation measurement at 7 mW pump power. At a fixed polarization angle of photon A (θ_A), coincidence counts between SPD1 and SPD2 over a 1 s interval are taken at different polarization angles of photon B (θ_B). Figure 3 shows the coincidence counts for $\theta_A = 0$ (circle dots) and $\theta_A = -\pi/4$ (square dots), and their sinusoidal fits. We use the Monte-Carlo method to calculate the visibilities of two interference fringes. The visibilities are $97.8\% \pm 1.5\%$ and $96.6\% \pm 2.2\%$ for $\theta_A = 0$ and $-\pi/4$, respectively. It should be noted that the visibilities decrease with increasing pump power. When the pump power is 20 mW, the visibilities decrease to 92%. The possible reason is that the large pump power causes the increase of multi-photon occurrence probability. We measure the Bell parameter S for the polarization-entangled photons at 7 mW pump power. In the canonical settings $\theta_A = 0$, $\theta'_A = \pi/4$, $\theta_B = \pi/8$, $\theta'_B = 3\pi/8$, we obtained an S value $S = 2.73 \pm 0.04$ which violates the Bell-CHSH inequality by ~18 standard deviations.

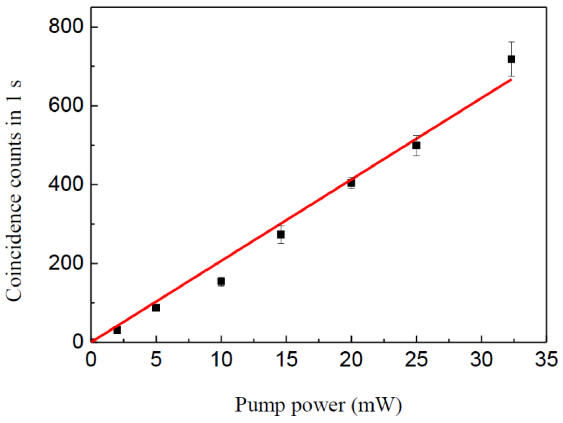

Fig. 2. (Color online) Coincidence counts in one second as a function of UV pump power. The black square dots are experimental data. The red line is the linear fitting.

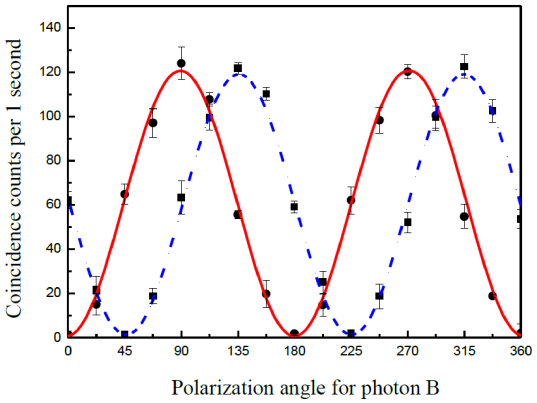

Fig. 3. (Color online) Coincidence counts for $\theta_A = 0$ (black circle dots) and $\theta_A = -\pi/4$ (black square dots) as a function of θ_B. The red (solid) and blue (dashed) curves are the sinusoidal fits to the experimental dates. The pump power is 7 mW.

In order to further quantify the quantum properties of produced entanglement source, we also perform a quantum state tomography. In the process, 16 coincidence counts of independent projection states are needed to determine the polarization state density matrix. We insert an additional QWP in front of each polarizer, so the photon A and B can be projected into arbitrary polarization state by rotating the angle of the QWPs and HWPs. Using the maximum likelihood estimation method[28,29] the density matrix is reconstructed as follows:

$$\rho = \begin{pmatrix} 0.0104 & -0.0323 - 0.0012i & -0.0012 - 0.0082i & -0.0019 + 0.0073i \\ -0.0323 + 0.0012i & 0.5055 & -0.4269 + 0.0331i & -0.0113 - 0.0199i \\ -0.0012 + 0.0082i & -0.4269 - 0.0331i & 0.4762 & 0.0162 - 0.0047i \\ -0.0019 - 0.0073i & -0.0113 + 0.0199i & 0.0162 + 0.0047i & 0.008 \end{pmatrix}. \quad (2)$$

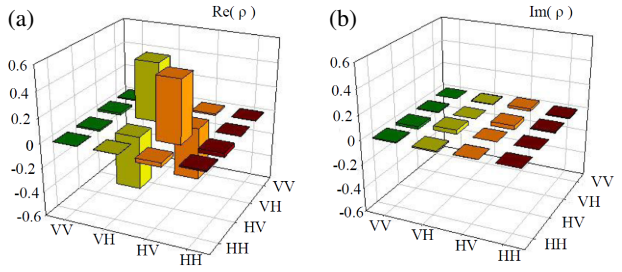

Fig. 4. (Color online) Real (a) and imaginary (b) parts of the density matrix of the generated entanglement photon pairs.

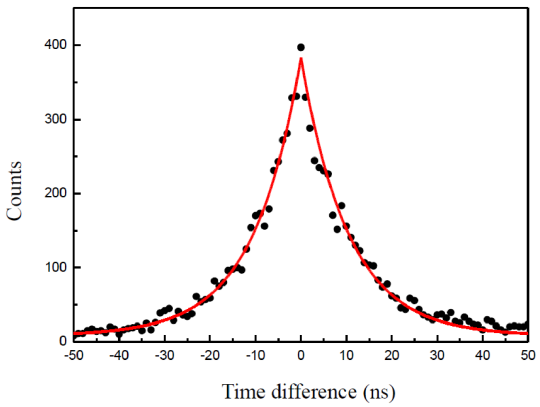

Fig. 5. (Color online) Measured time correlation between generated photon pairs. A function of $\exp(-2\pi\Delta\nu|t|)$ is used to fit the experimental data (black dots). The red curve is the fitted result.

Figures 4(a) and 4(b) show the real and imaginary parts of density matrix, respectively. By using the formula of $F = \sqrt{\langle\varphi|\rho|\varphi\rangle}$, we calculate the fidelity of reconstructed density matrix by comparing with the maximally entangled state $|\varphi\rangle = (1/\sqrt{2})(|H\rangle|V\rangle - |V\rangle|H\rangle)$, which amounts to $95.2\% \pm 0.8\%$.

The time correlation function between the generated photon pairs is measured to acquire the linewidth of the entanglement source. In the experiment, the detected signal of SPD1 is sent to the start channel of P7888, and the detected signal of SPD2 is sent to the stop channel of P7888. The resolution time of P7888 is set to 1 ns. By running the measurement 10000 times, we perform statistics of the counts in each time delay, and get the curve of counts vs time delay, as shown in Fig. 5. The FWHM of correlation time is 14.5 ns. We use the function $\exp(-2\pi\Delta\nu|t|)$ to fit the experimental data, the best fit shows that the linewidth ($\Delta\nu$) is about 15 MHz, which matches the typical atomic memory bandwidth.

In Fig. 5, as the event time digitizer P7888 have a resolution time of 1 ns which is large than the cavity round-trip time of 670 ps, the time correlation measurement cannot prove our source single-mode output. To ensure the single-mode property of the generated photons, we measure its coherence length through a single-photon interference experiment[30,31] by using an MZ interferometer. The setup of MZ interferometer is shown in Fig. 6(a). The $|H\rangle$ mode of the filtered photon pairs is sent to a fiber beam splitter which separates the field from input port into two equal parts at output 1 and output 2 ports. The two fields from output 1

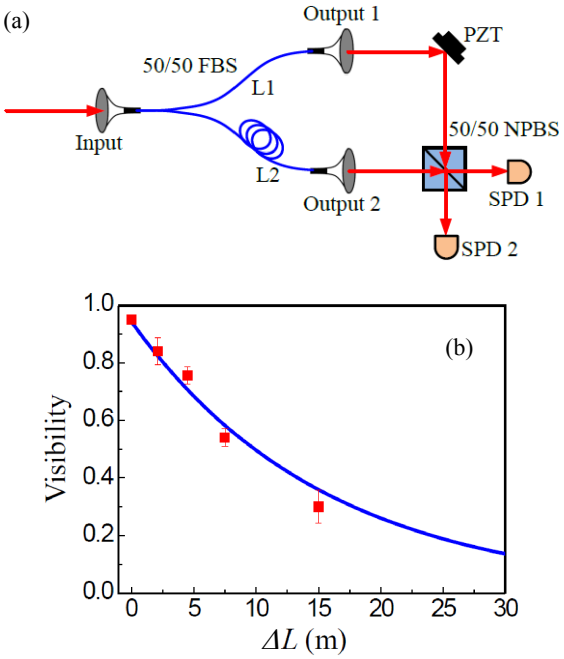

Fig. 6. (Color online) (a) Setup of MZ interferometer. 50/50 FBS: 50/50 fiber beam splitter; PZT: piozoelectric transducer; 50/50 NPBS: 50/50 non-polarizing beam splitter; SPD1–2: single photon detectors. (b) Measured visibility of the MZ interferometer versus its optical path difference. The data are fitted with a function of $V = V_0 \exp(-\Delta L/\Delta L_0)$. Error bars represent standard deviation.

and output 2 ports are combined with a 50/50 NPBS to form an MZ interferometer. To scan the interference fringes, a reflective mirror in one arm is attached with a piozoelectric transducer for fine tuning. With a classical light fed into the interferometer, an interference visibility of 0.97 is observed, showing the good quality of interferometer. To change the path difference between two arms, we cut the fiber L2 and connect the fibers with different lengths between two end-points. The measured visibilities versus the path difference between two interfering beams are shown in Fig. 6(b). The average interference visibility is 95% when the two arms have same lengths. The visibility declines with the increase of the path difference. When the path difference is 4.5 m, the visibility is still 75%. The coherence length is measured to be about 20 m, which is consistent with the result from the time correlation measurement in the relation of $\Delta L = \frac{\nu}{\Delta\nu}\lambda$, where ν and λ are the frequency and wavelength of SPDC photons, respectively. While for a multimode source, determined by the phase-matching condition, the coherence length is usually less than several mm. The measured coherence length provides good evidence that the generated photons are single-mode.

4. Conclusion

We report an experimental preparation of a narrow-band polarization-entangled photon pairs through cavity-enhanced SPDC. The wavelength of entangled source is 795 nm, corresponding to D1 line of Rb atoms. The single-mode photon pairs are selected by using multiple etalons as filters. The measured linewidth of entanglement source is 15 MHz which matches the typical atomic memory bandwidth. The measured bell parameter for the polarization-entangled photons $S = 2.73 \pm 0.04$ which violates the Bell-CHSH

inequality by ∼18 standard deviations. By performing quantum state tomography, we obtain fidelity of 95% between the generated entangled source and a maximally entangled state. The coherent length is measured to be about 20 m via an MZ interferometer. The presented entanglement source could be utilized in quantum communication and quantum computing based on quantum memories in atomic ensemble.

Acknowledgment

We acknowledge funding support from Key Project of the Ministry of Science and Technology of China (2016YFA0301402), the National Natural Science Foundation of China (Nos. 60821004, 11274211, and 10874106), the Program for Sanjin Scholars of Shanxi Province of China.

*lishujing@sxu.edu.cn
†wanghai@sxu.edu.cn

1) L. M. Duan, M. D. Lukin, J. I. Cirac, and P. Zoller, Nature **414**, 413 (2001).
2) N. Sangouard, C. Simon, H. de Riedmatten, and N. Gisin, Rev. Mod. Phys. **83**, 33 (2011).
3) E. Knill, R. Laflamme, and G. J. Milburn, Nature **409**, 46 (2001).
4) P. Kok, W. J. Munro, K. Nemoto, T. C. Ralph, J. P. Dowling, and G. J. Milburn, Rev. Mod. Phys. **79**, 135 (2007).
5) J. W. Pan, Z. B. Chen, C. Y. Lu, H. Weinfurter, A. Zeilinger, and M. Żukowski, Rev. Mod. Phys. **84**, 777 (2012).
6) D. Y. Cao, B. H. Liu, Z. Wang, Y. F. Huang, C. F. Li, and G. C. Guo, Sci. Bull. **60**, 1128 (2015).
7) D. C. Burnham and D. L. Weinberg, Phys. Rev. Lett. **25**, 84 (1970).
8) P. G. Kwiat, E. Waks, A. G. White, I. Appelbaum, and P. H. Eberhard, Phys. Rev. A **60**, R773 (1999).
9) P. G. Kwiat, K. Mattle, H. Weinfurter, A. Zeilinger, A. V. Sergienko, and Y. Shih, Phys. Rev. Lett. **75**, 4337 (1995).
10) F. König, E. J. Mason, F. N. C. Wong, and M. A. Albota, Phys. Rev. A **71**, 033805 (2005).
11) C. Clausen, I. Usmani, F. Bussières, N. Sangouard, M. Afzelius, H. de Riedmatten, and N. Gisin, Nature **469**, 508 (2011).
12) E. Saglamyurek, N. Sinclair, J. Jin, J. A. Slater, D. Oblak, F. Bussières, M. George, R. Ricken, W. Sohler, and W. Tittel, Nature **469**, 512 (2011).
13) Y. Wu, S. Li, W. Ge, Z. Xu, L. Tian, and H. Wang, Sci. Bull. **61**, 302 (2016).
14) K. Akiba, K. Kashiwagi, M. Arikawa, and M. Kozuma, New J. Phys. **11**, 013049 (2009).
15) K. F. Reim, J. Nunn, V. O. Lorenz, B. J. Sussman, K. C. Lee, N. K. Langford, D. Jaksch, and I. A. Walmsley, Nat. Photonics **4**, 218 (2010).
16) Y. A. Chen, S. Chen, Z. S. Yuan, B. Zhao, C. S. Chuu, J. Schmiedmayer, and J. W. Pan, Nat. Phys. **4**, 103 (2008).
17) A. I. Lvovsky, B. C. Sanders, and W. Tittel, Nat. Photonics **3**, 706 (2009).
18) D. G. England, P. S. Michelberger, T. F. M. Champion, K. F. Reim, K. C. Lee, M. R. Sprague, X. M. Jin, N. K. Langford, W. S. Kolthammer, J. Nunn, and I. A. Walmsley, J. Phys. B **45**, 124008 (2012).
19) Z. Y. Ou and Y. J. Lu, Phys. Rev. Lett. **83**, 2556 (1999).
20) H. B. Wang, T. Horikiri, and T. Kobayashi, Phys. Rev. A **70**, 043804 (2004).
21) C. E. Kuklewicz, F. N. C. Wong, and J. H. Shapiro, Phys. Rev. Lett. **97**, 223601 (2006).
22) M. Scholz, F. Wolfgramm, U. Herzog, and O. Benson, Appl. Phys. Lett. **91**, 191104 (2007).
23) F. Y. Wang, B. S. Shi, and G. C. Guo, Opt. Commun. **283**, 2974 (2010).
24) O. Morin, V. D'Auria, C. Fabre, and J. Laurat, Opt. Lett. **37**, 3738 (2012).
25) X. H. Bao, Y. Qian, J. Yang, H. Zhang, Z. B. Chen, T. Yang, and J. W. Pan, Phys. Rev. Lett. **101**, 190501 (2008).
26) H. Zhang, X. M. Jin, J. Yang, H. N. Dai, S. J. Yang, T. M. Zhao, J. Rui, Y. He, X. Jiang, F. Yang, G. S. Pan, Z. S. Yuan, Y. J. Deng, Z. B. Chen, X. H. Bao, S. Chen, B. Zhao, and J. W. Pan, Nat. Photonics **5**, 628 (2011).
27) R. W. P. Drever, J. L. Hall, F. V. Kowaiski, J. Hough, G. M. Ford, A. J. Munley, and H. Ward, Appl. Phys. B **31**, 97 (1983).
28) A. G. White, D. F. V. James, P. H. Eberhard, and P. G. Kwiat, Phys. Rev. Lett. **83**, 3103 (1999).
29) D. F. V. James, P. G. Kwiat, W. J. Munro, and A. G. White, Phys. Rev. A **64**, 052312 (2001).
30) J. Wang, P. Y. J. Lv, J. M. Cui, B. H. Liu, J. S. Tang, Y. F. Huang, C. F. Li, and G. C. Guo, Phys. Rev. Appl. **4**, 064011 (2015).
31) F. Y. Wang, B. S. Shi, C. Zhai, and G. C. Guo, J. Mod. Opt. **57**, 330 (2010).